Research Square

Preprints are preliminary reports that have not undergone peer review.
They should not be considered conclusive, used to inform clinical practice,
or referenced by the media as validated information.

Continents dry as declining precipitation efficiency redirects moisture pathways toward the ocean

Victoria Deman

Victoria.Deman@UGent.be

Ghent University https://orcid.org/0009-0002-0200-2408

Damián Insua-Costa

Ghent University https://orcid.org/0000-0001-9699-2806

João Geirinhas

Ghent University

Kirsten Findell

Geophysical Fluid Dynamics Laboratory https://orcid.org/0000-0002-1207-1637

Diego Miralles

Ghent University https://orcid.org/0000-0001-6186-5751

Article

Keywords:

Posted Date: November 4th, 2026

DOI: https://doi.org/10.21203/rs.3.rs-11386199/v1

License: This work is licensed under a Creative Commons Attribution 4.0 International License.
Read Full License

Additional Declarations: There is **NO** Competing Interest.

Continents dry as declining precipitation efficiency redirects moisture pathways toward the ocean

Victoria M. H. Deman[1*], Damián Insua-Costa[1], João Geirinhas[1], Kirsten L. Findell[2], Diego G. Miralles[1]

[1*]Hydro-Climate Extremes Lab, Ghent University, Ghent, Belgium.
[2]Geophysical Fluid Dynamics Laboratory, National Oceanic and Atmospheric Administration, Princeton, NJ, USA.

*Corresponding author(s). E-mail(s): victoria.deman@ugent.be;
Contributing authors: damian.insuacosta@ugent.be;
joao.marcelinogeirinhas@ugent.be; kirsten.findell@noaa.gov;
diego.miralles@ugent.be;

Abstract

Terrestrial water availability is declining across most regions, yet the underlying atmospheric processes remain unresolved. Here we show that this decline is dominated by a fall in the efficiency with which moisture precipitates over land, reorganizing land–ocean atmospheric moisture exchange. Combining a moisture tracking framework with a multi-dataset ensemble of precipitation and evaporation products for 1981–2023, we decompose this exchange into oceanic moisture import and continental moisture export. While oceanic evaporation increases and moisture transport toward land strengthens, a smaller fraction of this moisture precipitates over continents. Meanwhile, more continental moisture is exported to the oceans, further reducing continental precipitation recycling. Declining continental precipitation efficiency dominates these shifts, consistent with reduced relative humidity and increased atmospheric stability over land, linked to the land–ocean warming contrast and soil moisture limitation. These tendencies point to continued declines in continental water availability under warming, even as the global water cycle intensifies.

Water availability over land constrains ecosystems, food production, and socio-economic stability [1, 2]. Observations indicate that many regions have experienced declining soil moisture and increasing aridity in recent decades [3, 4], reshaping patterns of drought, heat stress and hydroclimatic extremes, and raising concerns about the vulnerability of continental water resources under continued warming [5]. At continental scales, terrestrial water availability is commonly assessed through trends in precipitation minus evaporation ($P - E$), which integrate the land–atmosphere water balance into a single net flux [6]. This quantity captures how much moisture a region gains or loses, but not the atmospheric pathways behind the change.

Global warming is expected to intensify the hydrological cycle through increased atmospheric moisture-holding capacity [7–9], yet this thermodynamic expectation alone does not explain the heterogeneous regional trends in water availability over land [10]. These have instead been attributed to shifts in precipitation and enhanced atmospheric evaporative demand under warming [5, 11, 12]; but precipitation and evaporation are themselves the integrated outcome of many interacting atmospheric and land–surface processes, including land–atmosphere coupling, circulation changes driven by greenhouse-gas forcing and climate variability, land–ocean warming contrasts, and aerosol effects [3, 8, 13–15]. Because these processes can reinforce or oppose one another, trends in $P - E$ record their net effect but cannot, on their own, reveal which mechanism dominates — or where the moisture that fails to precipitate over land instead goes.

Resolving this requires following the moisture itself. On timescales longer than seasonal, sustained shifts in continental $P - E$ must be balanced by atmospheric moisture convergence [13], and therefore by large-scale transport; because atmospheric circulation determines where evaporated moisture ultimately rains out, the transport pathway, and not the local flux alone, governs continental water availability.

Lagrangian moisture tracking makes these pathways explicit and enables their characterization using metrics such as precipitation recycling, the fraction of continental precipitation originating from continental evaporation, and evaporation recycling, the fraction of continental evaporation returning as precipitation over land [16–18]. Recent work shows that circulation changes can rival the influence of evaporation in reshaping continental precipitation recycling [19], while warming increasingly favours oceanic over continental evaporation as a source of continental precipitation [20]. Together, these advances show that both transport and surface fluxes reshape how moisture is redistributed between land and ocean, yet a unified account linking these changes back to the continental water balance is still lacking.

Combining Lagrangian moisture tracking simulations with a multi-dataset ensemble of precipitation and evaporation products for 1981–2023, we investigate the atmospheric processes underlying recent changes in continental $P - E$. We recast the terrestrial water balance as the difference between oceanic moisture import and continental moisture export and decompose changes along these pathways into contributions from evaporation, atmospheric transport and precipitation efficiency. This source–sink perspective reveals the processes governing changes in terrestrial water availability and their response to a warming climate.

1 Large-scale $P - E$ patterns and trends

The climatological mean $P - E$ for 1981–2023 (Fig. 1a) is characterized by large E and moisture divergence over the subtropical oceans balanced by large P and moisture convergence over most tropical land areas. This large-scale pattern is consistent with observed salinity distributions over the ocean [21]. However, trends in $P - E$ (Fig. 1b,c) differ between ocean and land. Over the ocean, divergence intensifies in already divergent regions and convergence strengthens in wet regions, consistent with thermodynamic expectations under warming and climate model projections [6, 22].

Over land, climatological $P - E$ is overall positive, reflecting the long-term balance in which mean P exceeds E and the surplus is returned to the oceans through runoff. Over the past four decades, however, it has declined, with the strongest decreases in South America, tropical Africa, and Southeast Asia, indicating reduced net water availability in these regions (Fig. 1b).

Whereas Fig. 1a,b are based on ERA5, Fig. 1c,d presents the global land $P - E$ trend across a large ensemble of dataset combinations, including ERA5 [23], ERA5-Land [24], MSWEPv2.8 [25], GPCP [26], GPCC [27], JRA-55 [28], FLUXCOM-X-BASE [29], and GLEAM v4.2 [30]. Across this ensemble, the mean and median trends are negative and statistically significant ($p < 0.05$; Fig. 1c,d). Of the 30 individual combinations, 22 show a negative trend and 10 a significant decline ($p < 0.05$), indicating a consistent drying signal. Although some products rely on ERA5 forcing (e.g., GLEAM and MSWEP), the negative trend is also evident in combinations based on largely independent gauge- and satellite-derived datasets, such as GPCC and GPCP. Thus, although trend magnitude varies among products (with ERA5 showing a stronger decline) the sign of the land-drying signal is unlikely to be an ERA5 artefact, supporting the use of ERA5 for subsequent analyses.

2 Drivers of land $P - E$ changes

To investigate the drivers of declining terrestrial water availability (1981–2023), we adopt a Lagrangian perspective on the atmospheric moisture budget. On multi-decadal timescales, changes in continental $P - E$ equal changes in vertically integrated atmospheric moisture convergence ($-\nabla \cdot Q$; Supplementary Fig. 1). However, the Eulerian moisture budget gives only the net flux across a region's boundaries, without distinguishing oceanic moisture from continental moisture transported in from upstream. Instead, by tracing atmospheric moisture from its source to its precipitation location, the Lagrangian framework partitions the moisture budget according to its origin

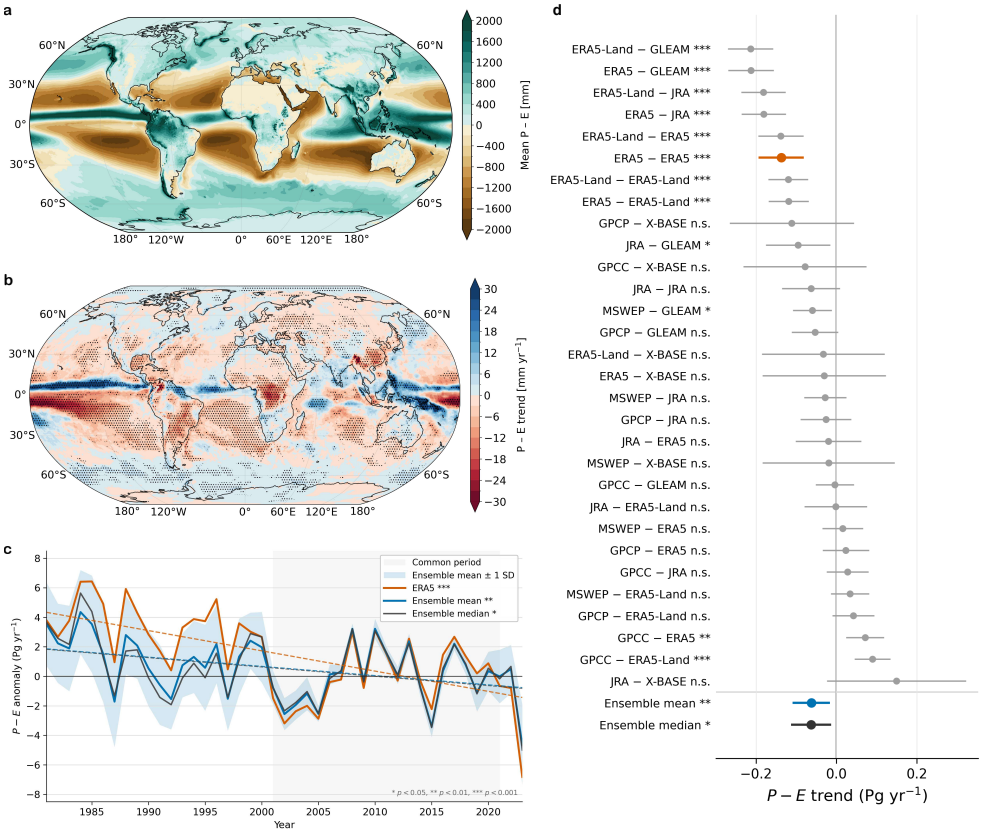


Fig. 1 Climatology and trends in terrestrial water availability. a, Climatological mean $P - E$ for 1981–2023 from ERA5. b, Spatial trend in $P - E$ for the same period, with stippling indicating significant trends ($p < 0.05$). c, Annual global land $P - E$ anomalies from ERA5 (orange) and the ensemble mean and median across all precipitation–evaporation dataset combinations (blue and black, respectively); blue shading indicates one standard deviation and grey shading the common period shared across all datasets. d, Linear trends in global land $P - E$ for each dataset combination, with whiskers indicating 95% confidence intervals; ERA5 and the ensemble statistics are coloured as in c. Trends are calculated over 1981–2023, except for combinations including FLUXCOM-X-BASE, which use its available period (2000–2021). Asterisks indicate statistical significance (*$p < 0.05$, **$p < 0.01$, ***$p < 0.001$).

and destination, directly linking changes in continental $P - E$ to shifts in moisture pathways.

We decompose precipitation (P) and evaporation (E) into their continental and oceanic components (denoted as Pc, Po, Ec and Eo) and further partition evaporation by where it precipitates: oceanic evaporation that precipitates over land (Eo2Pc),

oceanic evaporation that precipitates over the oceans (Eo2Po), continental evaporation that precipitates over land (Ec2Pc), and continental evaporation that precipitates over the oceans (Ec2Po). Over sufficiently long periods, for which atmospheric moisture storage changes are negligible relative to the fluxes, this expresses land $P - E$ as the balance between 'oceanic moisture import' (Eo2Pc) and 'continental moisture export' (Ec2Po):

$$P\mathrm{c} - E\mathrm{c} = (\mathrm{Ec2Pc} + \mathrm{Eo2Pc}) - (\mathrm{Ec2Pc} + \mathrm{Ec2Po}) = \mathrm{Eo2Pc} - \mathrm{Ec2Po} = -\nabla \cdot Q \quad (1)$$

As expected from Eq. 1, $P - E$ closely matches the diagnosed Lagrangian Eo2Pc−Ec2Po balance in the global time series (Supplementary Fig. 2).

Total evaporation increases over most ocean regions, while land evaporation trends are regionally variable (Fig. 2a). In contrast, evaporation contributing to continental precipitation (E2Pc=Ec2Pc+Eo2Pc) declines across major land regions (Fig. 2b), whereas evaporation contributing to ocean precipitation (E2Po=Ec2Po+Eo2Po) displays predominantly positive trends over land (Fig. 2c). In regions such as northern South America and tropical Africa, decreasing E2Pc coincides with increasing E2Po, indicating that a growing fraction of continental evaporation is exported to the oceans rather than recycled over land, consistent with previous modelling studies [20].

Quantitatively, both reduced oceanic moisture import and increased continental moisture export contribute to declining land $P - E$. Approximately 62% of the trend is associated with a reduction in ocean-to-land import (Eo2Pc), and the remaining 38% with increased continental export (Ec2Po) (Supplementary Fig. 2). This asymmetry reflects the larger magnitude of Eo2Pc than Ec2Po, such that absolute changes in oceanic moisture import exert a stronger influence on land $P - E$. The two changes also carry different spatial signatures: reduced Eo2Pc would concentrate drying near

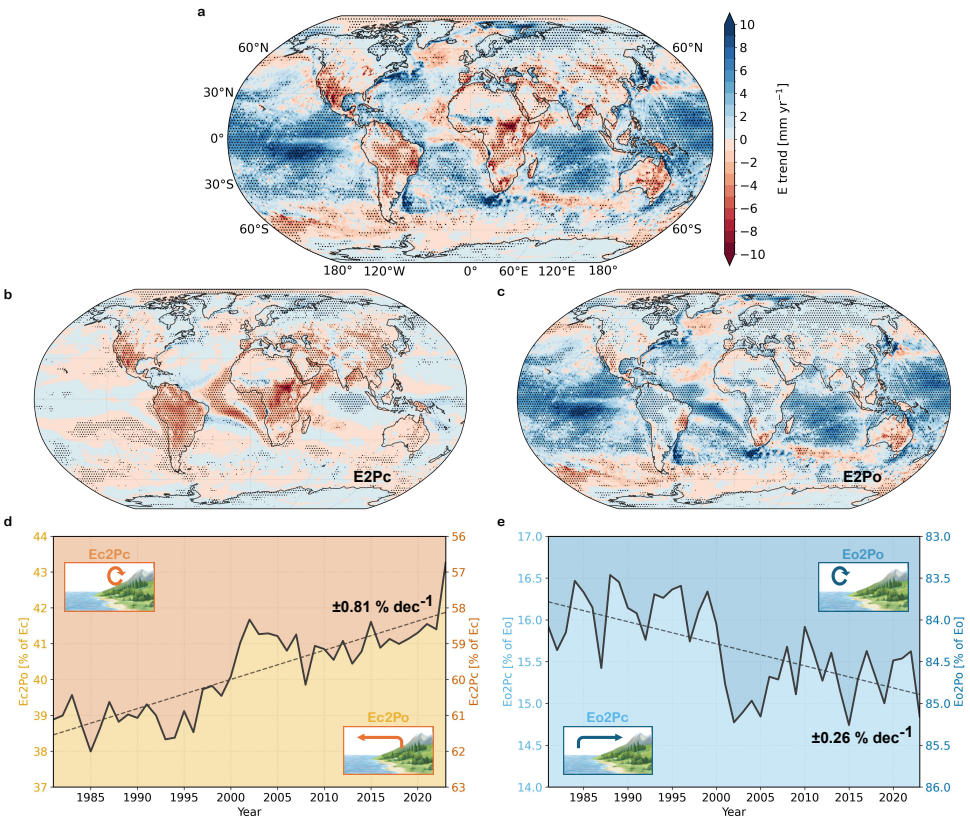


Fig. 2 Changes in the land–ocean partitioning of evaporation. a, Trend in total evaporation E. b, Trend in evaporation contributing to continental precipitation (E2Pc). c, Trend in evaporation contributing to ocean precipitation (E2Po). d, Fraction of land evaporation precipitating over land ($\frac{\text{Ec2Pc}}{Ec}$) and ocean ($\frac{\text{Ec2Po}}{Ec}$). e, Fraction of ocean evaporation precipitating over land ($\frac{\text{Eo2Pc}}{Eo}$) and ocean ($\frac{\text{Eo2Po}}{Eo}$).

coasts and downwind moisture-entry regions, where oceanic supply dominates, whereas increased Ec2Po would preferentially amplify drying over continental interiors, which depend more on recycled moisture. In relative terms, however, the redistribution of continental evaporation is stronger: the fraction of continental evaporation exported to the oceans (Ec2Po/Ec) increases by 0.81% per decade (Fig. 2d), with increases widespread across continental regions (Supplementary Fig. 3), implying a corresponding decline in continental evaporation recycling (Ec2Pc/Ec), whereas the imported fraction (Eo2Pc/Eo) decreases by only 0.26% per decade (Fig. 2e). Thus, although

Ec2Po explains a smaller fraction of the absolute $P - E$ trend, it exhibits the larger fractional change.

Continental precipitation recycling (Ec2Pc/Pc) also declines, by 0.57% per decade (Supplementary Fig. 4), indicating a reduced contribution of land evaporation to total precipitation over land. The precipitation and evaporation recycling trends computed by Findell et al. [20] using GFDL–ESM2G are comparable in magnitude and direction to those found here using ERA5 (Fig. 2d and Supplementary Fig. 4), despite methodological differences, supporting this shift in land–ocean moisture partitioning.

3 Decomposing the moisture pathways

The amount of moisture transferred from a source to a sink can be altered by processes acting at the source, during atmospheric transport, or at the destination. To isolate the mechanisms underlying the declining $P-E$, we decompose trends in Ec2Po and Eo2Pc into contributions from changes in E (Fig. 3d,h) and three partitioning factors (α, β, γ; see Methods), representing successive stages of the pathway from evaporation to precipitation. The factor α (Fig. 3a,e) is moisture pathway connectivity, i.e. the fraction of evaporated moisture that is embedded in trajectories reaching the sink, independent of precipitation along the path. β (Fig. 3b,f) is *en route* survival, the fraction of transported moisture that survives precipitation before reaching the sink. Finally, γ (Fig. 3c,g) is precipitation efficiency within the sink region (land or ocean), i.e. how efficiently the available moisture over the sink is converted into precipitation. Here, precipitation efficiency denotes the climatological conversion of atmospheric moisture into precipitation, rather than the precipitation efficiency of individual weather events governed by local storm-scale processes such as convection and cloud microphysics.

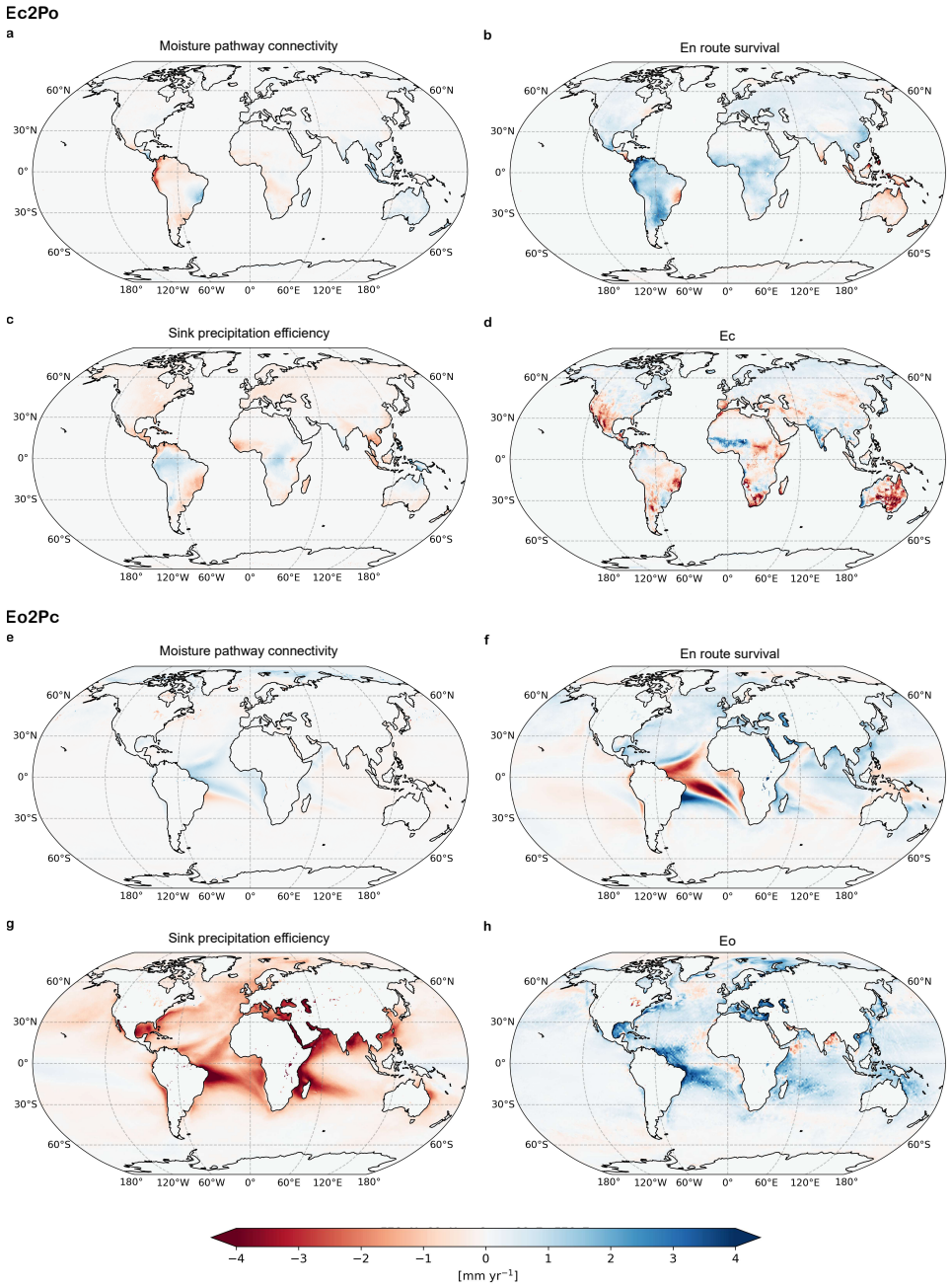


Fig. 3 Decomposition of trends in moisture pathways. Panels (a–d) show contributions to trends in export (Ec2Po): a, Moisture pathway connectivity (α), b, *En route* survival (β), c, Sink precipitation efficiency (γ), and d, Source evaporation over land (Ec). Panels (e–h) show the corresponding contributions to trends in import (Eo2Pc): e, α, f, β, g, γ, and h, Source evaporation over the ocean (Eo).

For continental moisture export (Ec2Po), the decomposition (Supplementary Table 1) shows that the positive trend (Fig. 2d) is not driven by enhanced continental evaporation itself; in fact, the direct contribution from Ec is negative (–0.21 mm dec^{-1}), which on its own would reduce Ec2Po and favour a stabilization or increase in $P - E$. This negative ERA5 land evaporation trend contrasts with the predominantly positive trends reported in the literature [31]. Instead, the increase in Ec2Po is led by an increase in β (0.84 mm dec^{-1}). This indicates reduced upstream rainout along these pathways, allowing more land-derived moisture to survive transport and reach the ocean. The smaller increase in α indicates that a larger share of continental evaporation is embedded in trajectories that reach oceanic sinks. Changes in γ over ocean sinks are small and slightly negative, implying that oceanic precipitation efficiency does not drive the increase.

In contrast, oceanic moisture import (Eo2Pc) declines (Fig. 2e) despite increases in ocean evaporation and positive contributions from α and β (together 3.42 mm dec^{-1}), which imply increased supply, connectivity, and *en route* survival. The dominant driver of the decline is a pronounced reduction in γ (–4.05 mm dec^{-1}) over continental sinks. Thus, although more moisture reaches the continents, a smaller fraction precipitates there.

Both branches (Ec2Po and Eo2Pc) point to the same driver: a declining continental precipitation efficiency, expressed through increased β for Ec2Po and through decreased γ for Eo2Pc. Consistent with this, a trajectory-independent Eulerian diagnostic of continental precipitation efficiency, the ratio of precipitation to total column water, shows negative trends over most land areas (Supplementary Fig. 5), where warming generally exceeds that over the oceans.

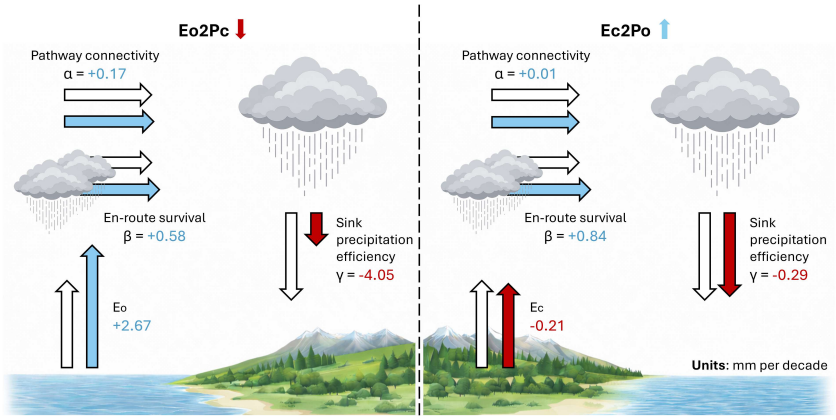


Fig. 4 Conceptual summary of changes in atmospheric moisture pathways. Schematic of the mechanisms driving declining land $P - E$. Left: ocean-to-land moisture import (Eo2Pc) decreases despite increasing ocean evaporation, due to reduced precipitation efficiency over land (γ), which outweighs increases in pathway connectivity (α) and *en route* survival (β). Right: land-to-ocean export (Ec2Po) increases primarily due to reduced upstream rainout (β), despite declining continental evaporation (Ec). Together, these changes indicate a shift toward increased export of continental moisture and reduced recycling over land. White arrows represent the original moisture pathway, while coloured arrows show the resulting pathway after the diagnosed changes. Numbers give the contribution of each component to the trend in mm per decade.

4 Regional manifestations of moisture transport changes

Regional patterns illustrate how these mechanisms manifest within key circulation systems. Although at the global scale the decline in precipitation efficiency is the dominant driver of continental drying, at the regional scale other components such as changes in atmospheric circulation can be equally or more relevant. The examples below highlight the dominant process in each region.

In southeastern South America and along the South American Low-Level Jet (SALLJ) corridor, positive β trends for Ec2Po (Fig. 3b) indicate enhanced survival of continental moisture during export toward the South Atlantic, consistent with reported increases in SALLJ wind speeds and a poleward shift of the South Atlantic convergence zone [32, 33]. For Ec2Po, increases in γ (Fig. 3c) for moisture originating

from the Amazon and Congo basins reflect enhanced precipitation efficiency over tropical oceanic sinks, likely driven by enhanced convection and moisture convergence over the warming tropical oceans, promoting rainout of transported continental moisture [34]. Conversely, decreases in Ec2Po over southwestern North America, southern Africa and Australia (Fig. 2c) are dominated by reduced continental evaporation (Fig. 3d), consistent with reported drying in those regions [35, 36].

Central-eastern South America exhibits opposing α and β trends (Fig. 3a,b), with strengthened connectivity to ocean sinks (positive α) partially offset by increased *en route* precipitation (negative β). At the same time, the negative Ec contribution (Fig. 3d) indicates reduced continental moisture supply, consistent with regional drying. These patterns align with enhanced anticyclonic circulation over central-eastern South America associated with cold-phase ENSO and PDO conditions [37–39]. Stronger winds may enhance pathway connectivity, while altered transport through inland convergence zones could increase *en route* rainout before moisture reaches the coast.

For Eo2Pc, enhanced *en route* precipitation over the central tropical Atlantic reduces the oceanic moisture reaching South America (Fig. 3f). Again, this pattern is consistent with cold-phase ENSO and PDO circulation anomalies. Cold eastern equatorial Pacific sea surface temperatures (SSTs), together with warm SSTs and enhanced diabatic heating over the western equatorial Atlantic, strengthen the ascending branch of the Walker cell over this region of the Atlantic and surrounding land areas. This intensifies moisture convergence and convection in the lower troposphere, promoting precipitation along the trade-wind pathway, and thereby explaining the negative β trend [38, 40, 41]. On the flanks of the core convergence zone, β increases, indicating greater moisture survival. Stronger trade winds simultaneously enhance mass transport consistent with positive α trends (Fig. 3e). Together, these patterns suggest a reorganization of tropical Atlantic–South American moisture transport, consistent

with long-term circulation changes [38]. The β pattern is also consistent with a narrowing and intensification of the Atlantic ITCZ, with enhanced rainout near its core and greater moisture survival on its flanks [34].

5 Discussion

By reformulating the continental water budget as a balance between oceanic moisture import and continental moisture export, we provide a source–sink perspective on terrestrial water availability. Continental drying reflects both declining oceanic moisture import and increasing continental moisture export. Our decomposition shows that both changes are dominated by a declining precipitation efficiency over land: less ocean-derived moisture precipitates over land, while more continental moisture survives transport and is exported to the oceans (Fig. 4).

Several thermodynamic mechanisms can explain the observed decline in continental precipitation efficiency. Under warming, atmospheric water vapour increases approximately following Clausius–Clapeyron scaling, whereas precipitation is constrained by the atmospheric energy budget and cannot increase proportionally [42–44]. Therefore, atmospheric moisture is removed more slowly, increasing residence times and transport distances [45]. However, this global constraint alone cannot explain why precipitation efficiency declines more strongly over land than over oceans. The land–ocean warming contrast provides a mechanism for this continental amplification. Despite similar increases in moist static energy over neighbouring land and ocean regions, limited moisture availability over drier land favours sensible heating and stronger warming [13, 34]. Although moisture transport toward land strengthens (Fig. 4), continental specific humidity cannot keep pace with increasing saturation point. The resulting decline in relative humidity makes ocean-derived moisture less likely to precipitate after reaching land, explaining the declining γ for Eo2Pc (Fig. 4).

However, the land–ocean warming contrast acts primarily on ocean-to-land transport and does not fully explain the greater survival of continental moisture exported toward the oceans. Soil moisture limitation provides an additional mechanism. As evaporative demand outpaces precipitation, drying soils constrain evaporation and prevent near-surface humidity from keeping pace with warming [46], while shifting surface energy from latent to sensible heating and further amplifying land warming [47]. The resulting decline in relative humidity suppresses precipitation by raising the lifting condensation level. Increased atmospheric stability from preferential upper-tropospheric warming associated with latent heat release further inhibits precipitation [42, 48]. Consistent with this interpretation, Dong et al. [49] report fewer mesoscale convective systems over tropical land as SSTs rise. Together, these interacting atmospheric and land–surface processes reduce precipitation efficiency over land for both oceanic and continental moisture, consistent with the changes identified in both pathways.

Previous studies attributed declining continental precipitation recycling to soil moisture limitation that constrains continental evaporation, thereby increasing the relative contribution of oceanic moisture [20]. Our results reveal an additional pathway: soil moisture limitation also reduces relative humidity and precipitation efficiency over land, allowing a larger fraction of continental moisture to remain airborne and be exported to the oceans. Thus, declining precipitation recycling reflects not only reduced continental evaporation, but also reduced retention of continental moisture over land.

The thermodynamic framework outlined above explains the overall decline in continental precipitation efficiency, but not its regional heterogeneity. Regional departures also reflect changes in atmospheric circulation and internal variability. Circulation changes can simultaneously alter moisture transport pathways and precipitation processes, such that the α, β, and γ terms are not fully independent. Moreover, trends

reflect the superposition of long-term circulation adjustments and multi-decadal internal variability, which influence atmospheric moisture transport on similar timescales. Recent decades have been characterized by predominantly cold-phase ENSO and PDO conditions (Supplementary Fig. 6), potentially contributing to the identified patterns over South America and central Africa. If these circulation changes are externally forced by anthropogenic emissions, the reported decline in net water availability across these regions is likely to persist. Conversely, if they primarily reflect internal climate variability at decadal scales, future circulation changes could partially offset the thermodynamically driven drying from the land–ocean warming contrast and soil moisture limitation [50]. Disentangling forced responses from internal variability and isolating the underlying dynamical mechanisms therefore remains a priority. Finally, while the sign of the land $P-E$ decline is robust across independent datasets (Fig. 1c), the mechanistic decomposition relies on ERA5-driven trajectories and ERA5 surface fluxes. The magnitudes of the α, β, and γ contributions may therefore carry reanalysis-specific biases, motivating replication with independent reanalyses (e.g. JRA-55, MERRA-2).

Future terrestrial drying depends not only on the amount of atmospheric moisture, but also on its fate. Declining continental precipitation efficiency increasingly redirects moisture away from land, weakening the terrestrial branch of the hydrological cycle despite its overall intensification. By moving from net moisture convergence to explicit source–sink relationships, our framework provides a process-based perspective on terrestrial drying that links observed changes in atmospheric moisture pathways directly to the underlying physical mechanisms. This perspective offers a basis for anticipating future changes in continental water availability beyond precipitation and evaporation trends alone.

6 Methods

6.1 FLEXPART trajectory simulations

Atmospheric transport was analysed using a global archive of Lagrangian air-parcel trajectories generated with the FLEXible PARTicle dispersion model (FLEXPART v11; 51). FLEXPART calculates the three-dimensional motion of air parcels based on large-scale meteorological fields, with additional parametrizations representing unresolved turbulence and convection. The simulations are driven by the ERA5 reanalysis [23], which provides a globally complete and dynamically consistent atmospheric state with stable quality over the satellite era, making it suitable for long-term transport analyses.

FLEXPART was run in domain-filling mode, releasing approximately 20 million equally weighted air parcels per year and sampling the troposphere at 3-hourly resolution. The resulting trajectories provide time-resolved parcel positions, and dynamic and thermodynamic properties, which form the basis for the source–sink diagnostics applied here. Full details of the FLEXPART configuration and trajectory dataset are provided in Deman et al. [52].

6.2 Moisture source–sink diagnostics

Source–sink relationships for atmospheric moisture were diagnosed using the Heat And MoiSture Tracking framEwoRk (HAMSTER v2; 52, 53). HAMSTER analyses changes in specific humidity along FLEXPART trajectories to identify where air parcels gain or lose moisture through surface exchange processes.

We apply HAMSTER in backward mode to trace precipitation in each sink back to its surface moisture sources over a 30-day period. The resulting evaporation-to-precipitation (E2P) field quantifies the amount of evaporation that ultimately precipitates within the sink of interest. This window exceeds the typical atmospheric

moisture residence time and captures both local and remote sources. We consider two sinks covering the entire globe: all continents (E2Pc) and all oceans (E2Po).

A central feature of HAMSTER v2 is a dynamic bias-correction scheme applied *en route* along parcel trajectories. At each time step, diagnosed moisture and heat tendencies are rescaled to match ERA5 surface E and P, ensuring physical consistency with the driving reanalysis. This correction accounts for the fact that trajectory-based parcel tendencies reflect only the net effect of unresolved surface exchange processes and transport. A final rescaling ensures consistency with ERA5 evaporation and precipitation. Owing to the 30-day backtracking window, analyses are restricted to 1981–2023. Further details on the HAMSTER methodology, updates in version 2, and framework evaluation are provided in Deman et al. [52].

6.3 Linear decomposition of E2P

To disentangle the drivers of changes in E2P, we adopt and extend the linear decomposition framework of Li et al. [54]. We decompose E2P into four multiplicative components representing evaporation supply, moisture pathway connectivity, *en route* moisture survival, and precipitation conversion within the sink. Specifically, we write:

$$E2P = \frac{E2Q_{nodisc}}{E} \cdot \frac{E2Q}{E2Q_{nodisc}} \cdot \frac{E2P}{E2Q} \cdot E = \alpha \cdot \beta \cdot \gamma \cdot E \tag{2}$$

where E denotes source evaporation, $E2Q_{nodisc}$ represents the potential moisture availability over the sink assuming no rainout along trajectories (i.e., without discounting moisture losses during transport), $E2Q$ represents realized moisture availability over the sink after accounting for upstream losses, and $E2P$ denotes precipitation over the sink attributable to the source.

The three dimensionless factors are defined as:

$$\alpha = \frac{E2Q_{nodisc}}{E}; \quad \beta = \frac{E2Q}{E2Q_{nodisc}}; \quad \gamma = \frac{E2P}{E2Q} \tag{3}$$

These factors have the following interpretations:

α: Moisture pathway connectivity. It quantifies the fraction of evaporated moisture that is embedded in trajectories reaching the sink, independent of rainout along the path. It represents a moisture-weighted measure of atmospheric connectivity between source and sink, closely related to the underlying air transport rather than the amount of source moisture carried.

β: *En route* survival fraction. It measures the fraction of potentially transported moisture that survives upstream rainout and dilution before reaching the sink.

γ: Sink precipitation efficiency. It quantifies how efficiently available moisture over the sink is converted into precipitation.

All quantities are computed at seasonal resolution (DJF, MAM, JJA, SON) and subsequently combined into annual values, which avoids biases arising from covariance between factors and evaporation when using annual means. Assuming that $E2P = \alpha \cdot \beta \cdot \gamma \cdot E$, the temporal derivative follows from the product rule:

$$\frac{\partial E2P}{\partial t} = \frac{\partial \alpha}{\partial t} \cdot \beta \cdot \gamma \cdot E + \frac{\partial \beta}{\partial t} \cdot \alpha \cdot \gamma \cdot E + \frac{\partial \gamma}{\partial t} \cdot \alpha \cdot \beta \cdot E + \frac{\partial E}{\partial t} \cdot \alpha \cdot \beta \cdot \gamma \tag{4}$$

Taking linear trends over time, we obtain:

$$S_{E2P} = S_\alpha \cdot \overline{\beta} \cdot \overline{\gamma} \cdot \overline{E} + S_\beta \cdot \overline{\alpha} \cdot \overline{\gamma} \cdot \overline{E} + S_\gamma \cdot \overline{\alpha} \cdot \overline{\beta} \cdot \overline{E} + S_E \cdot \overline{\alpha} \cdot \overline{\beta} \cdot \overline{\gamma} + \delta \tag{5}$$

where S_{E2P}, S_E, S_α, S_β, S_γ are the slopes of the linear regression (trend) of E2P, E, α, β, γ, overbars indicate mean values over the same period, and δ represents the residual associated with higher-order covariance terms neglected in the first-order approximation. The approximation corresponds to a first-order Taylor expansion around the mean state, whereby higher-order covariance and interaction terms are neglected. As the residual term is small (Supplementary Fig. 7 and Supplementary Table 1; 0.8% of

total for Eo2Pc and 1.1% of total for Ec2Pc), this linear approximation captures the total trend.

Declarations

Data availability. ERA5 and ERA5-Land reanalysis data [23, 24] were obtained from the Copernicus Climate Data Store (CDS) and are publicly available at https://cds.climate.copernicus.eu/. Flex_extract software (https://flexpart.img.univie.ac.at/flexextract/) was used to retrieve these meteorological fields from the ECMWF.

MSWEP v2.8 [25] data are available at https://www.gloh2o.org/, GPCP [26] data at https://psl.noaa.gov/data/gridded/data.gpcp.html, GPCC [27] data at https://opendata.dwd.de/climate_environment/GPCC/GPCC_Precipitation_Analysis_Monthly/Version_2025/050_degree/, GLEAM v4.2a [30] data at https://www.gleam.eu/. FLUXCOM-X-BASE [29] data at https://meta.icos-cp.eu/collections/_l85vWiIV81AifoxCkty50YI, and JRA-55 [28] data at https://www.data.jma.go.jp/jra/html/JRA-55/index_en.html.

Code availability. The FLEXPART model source code is openly available at https://www.flexpart.eu/. The FLEXPART–ERA5 trajectory output used in this study is hosted at Globus (https://app.globus.org/file-manager?origin_id=269ce146-5835-4e3c-91d0-f37c9166c52a&origin_path=%2F) and archived on Zenodo (https://doi.org/10.5281/zenodo.17952362, 55). The source code for HAMSTER v2 is archived on Zenodo [53] and openly available at https://github.com/h-cel/HAMSTER-v2.

Acknowledgements. The computational resources and services used in this work were provided by the VSC (Flemish Supercomputer Center), funded by the FWO and the Flemish Government, Department of Economy, Science and Innovation (EWI). D.G.M., J.G. and V.M.H.D. acknowledge support from the European Research Council (ERC) Consolidator grant HEAT (101088405). D.I.C. acknowledges funding from the

Bijzonder Onderzoeksfonds (BOF) from Ghent University (BOF24/PDO/ 027). AI-assisted language tools were used to improve the clarity of the manuscript.

Author contributions. D.G.M, D.I.C. and V.M.H.D. conceived the study. V.M.H.D. performed the FLEXPART simulations and the additional analyses. All authors contributed to the writing of the manuscript and the interpretation of the results.

Conflict of interest. The authors declare no competing interests.

References

[1] Fitton, N. *et al.* The vulnerabilities of agricultural land and food production to future water scarcity. *Global Environmental Change* **58**, 101944 (2019).

[2] WWAP (UNESCO World Water Assessment Programme). The United Nations World Water Development Report 2019: Leaving No One Behind. Paris, UNESCO (2019).

[3] Greve, P. & Seneviratne, S. I. Assessment of future changes in water availability and aridity. *Geophysical Research Letters* **42**, 5493–5499 (2015).

[4] Sardans, J. *et al.* Growing aridity poses threats to global land surface. *Communications Earth & Environment* **5**, 776 (2024).

[5] IPCC. in *Chapter 8: Water Cycle Changes* (eds Masson-Delmotte, V. *et al.*) *Climate Change 2021: The Physical Science Basis. Contribution of Working Group I to the Sixth Assessment Report of the Intergovernmental Panel on Climate Change* 1055–1210 (Cambridge University Press, Cambridge, United Kingdom and New York, NY, USA, 2021). URL https://www.ipcc.ch/report/ar6/wg1/chapter/chapter-8/.

[6] Held, I. M. & Soden, B. J. Robust responses of the hydrological cycle to global warming. *Journal of Climate* **19**, 5686–5699 (2006).

[7] Ficklin, D. L., Null, S. E., Abatzoglou, J. T., Novick, K. A. & Myers, D. T. Hydrological intensification will increase the complexity of water resource management. *Earth's Future* **10**, e2021EF002487 (2022).

[8] Zaitchik, B. F., Rodell, M., Biasutti, M. & Seneviratne, S. I. Wetting and drying trends under climate change. *Nature Water* **1**, 502–513 (2023).

[9] Ehtasham, L., Sherani, S. H. & Nawaz, F. Acceleration of the hydrological cycle and its impact on water availability over land: an adverse effect of climate change. *Meteorology Hydrology and Water Management. Research and Operational Applications* **12** (2024).

[10] Greve, P. *et al.* Global assessment of trends in wetting and drying over land. *Nature Geoscience* **7**, 716–721 (2014).

[11] Vicente-Serrano, S. M., McVicar, T. R., Miralles, D. G., Yang, Y. & Tomas-Burguera, M. Unraveling the influence of atmospheric evaporative demand on drought and its response to climate change. *Wiley Interdisciplinary Reviews: Climate Change* **11**, e632 (2020).

[12] Padrón, R. S. *et al.* Observed changes in dry-season water availability attributed to human-induced climate change. *Nature Geoscience* **13**, 477–481 (2020).

[13] Byrne, M. P. & O'Gorman, P. A. The response of precipitation minus evapotranspiration to climate warming: Why the "wet-get-wetter, dry-get-drier" scaling does not hold over land. *Journal of Climate* **28**, 8078–8092 (2015).

[14] Roderick, M. L., Sun, F., Lim, W. H. & Farquhar, G. D. A general framework for understanding the response of the water cycle to global warming over land and ocean. *Hydrology and Earth System Sciences* **18**, 1575–1589 (2014).

[15] Shepherd, T. G. Atmospheric circulation as a source of uncertainty in climate change projections. *Nature Geoscience* **7**, 703–708 (2014).

[16] Eltahir, E. A. B. & Bras, R. L. Precipitation recycling. *Reviews of Geophysics* **34**, 367–378 (1996).

[17] Van der Ent, R. J., Savenije, H. H., Schaefli, B. & Steele-Dunne, S. C. Origin and fate of atmospheric moisture over continents. *Water Resources Research* **46** (2010).

[18] Gimeno, L., Nieto, R. & Sorí, R. The growing importance of oceanic moisture sources for continental precipitation. *npj Climate and Atmospheric Science* **3**, 27 (2020).

[19] Cui, J., Lian, X., van der Ent, R. J., Gimeno, L. & Miralles, D. G. Greater role of atmospheric circulation than evapotranspiration in reshaping terrestrial moisture recycling. *Science Bulletin* (2026).

[20] Findell, K. L. *et al.* Rising temperatures increase importance of oceanic evaporation as a source for continental precipitation. *Journal of Climate* **32**, 7713–7726 (2019).

[21] Zika, J. D. *et al.* Improved estimates of water cycle change from ocean salinity: The key role of ocean warming. *Environmental Research Letters* **13**, 074036 (2018).

[22] Durack, P. J., Wijffels, S. E. & Matear, R. J. Ocean salinities reveal strong global water cycle intensification during 1950 to 2000. *Science* **336**, 455–458 (2012).

[23] Hersbach, H. *et al.* The ERA5 global reanalysis. *Quarterly Journal of the Royal Meteorological Society* **146**, 1999–2049 (2020).

[24] Muñoz-Sabater, J. *et al.* ERA5-Land: A state-of-the-art global reanalysis dataset for land applications. *Earth System Science Data* **13**, 4349–4383 (2021).

[25] Beck, H. E. *et al.* MSWEP V2 global 3-hourly 0.1 precipitation: methodology and quantitative assessment. *Bulletin of the American Meteorological Society* **100**, 473–500 (2019).

[26] Adler, R. F. *et al.* The version-2 global precipitation climatology project (GPCP) monthly precipitation analysis (1979–present). *Journal of Hydrometeorology* **4**, 1147–1167 (2003).

[27] Schneider, U. *et al.* GPCC full data reanalysis version 7.0: monthly land-surface precipitation from rain gauges built on GTS based and historic data (2016).

[28] Kobayashi, S. *et al.* The JRA-55 reanalysis: General specifications and basic characteristics. *Journal of the Meteorological Society of Japan. Ser. II* **93**, 5–48 (2015).

[29] Nelson, J. A. *et al.* X-BASE: the first terrestrial carbon and water flux products from an extended data-driven scaling framework, FLUXCOM-X. *Biogeosciences* **21**, 5079–5115 (2024).

[30] Miralles, D. G. *et al.* GLEAM4: global land evaporation and soil moisture dataset at 0.1 resolution from 1980 to near present. *Scientific Data* **12**, 416 (2025).

[31] Tang, R. *et al.* Spatial-temporal patterns of land surface evapotranspiration from global products. *Remote Sensing of Environment* **304**, 114066 (2024).

[32] Montini, T. L., Jones, C. & Carvalho, L. M. The South American low-level jet: A new climatology, variability, and changes. *Journal of Geophysical Research: Atmospheres* **124**, 1200–1218 (2019).

[33] Zilli, M. T., Carvalho, L. M. & Lintner, B. R. The poleward shift of South Atlantic Convergence Zone in recent decades. *Climate Dynamics* **52**, 2545–2563 (2019).

[34] Byrne, M. P., Pendergrass, A. G., Rapp, A. D. & Wodzicki, K. R. Response of the intertropical convergence zone to climate change: Location, width, and strength. *Current climate change reports* **4**, 355–370 (2018).

[35] Luo, D. *et al.* An overall consistent increase of global aridity in 1970–2018. *Journal of Geographical Sciences* **33**, 449–463 (2023).

[36] Li, S. *et al.* Increasing vapor pressure deficit accelerates land drying. *Journal of Hydrology* **625**, 130062 (2023).

[37] Silva, M. E. S., Silva, C. B., Ambrizzi, T., Drumond, A. & Patucci, N. N. South America climate during the 1970–2001 Pacific Decadal Oscillation phases based on different reanalysis datasets. *Frontiers in Earth Science* **7**, 359 (2020).

[38] Geirinhas, J. *et al.* Combined large-scale tropical and subtropical forcing on the severe 2019–2022 drought in South America. *npj Climate and Atmospheric Science* **6**, 185 (2023).

[39] Mu, Y. *et al.* Pacific decadal oscillation and ENSO forcings of northerly low-level jets in South America. *npj Climate and Atmospheric Science* **7**, 297 (2024).

[40] Sasaki, W., Doi, T., Richards, K. J. & Masumoto, Y. The influence of ENSO on the equatorial Atlantic precipitation through the Walker circulation in a CGCM. *Climate Dynamics* **44**, 191–202 (2015).

[41] Cai, W. *et al.* Climate impacts of the El Niño–southern oscillation on South America. *Nature Reviews Earth & Environment* **1**, 215–231 (2020).

[42] Allen, M. R. & Ingram, W. J. Constraints on future changes in climate and the hydrologic cycle. *Nature* **419**, 224–232 (2002).

[43] Pendergrass, A. G. & Hartmann, D. L. The atmospheric energy constraint on global-mean precipitation change. *Journal of Climate* **27**, 757–768 (2014).

[44] O'Gorman, P. A., Allan, R. P., Byrne, M. P. & Previdi, M. Energetic constraints on precipitation under climate change. *Surveys in Geophysics* **33**, 585–608 (2012).

[45] Gimeno, L. *et al.* The residence time of water vapour in the atmosphere. *Nature Reviews Earth Environment* **2**, 558–569 (2021).

[46] Zhou, W., Leung, L. R. & Lu, J. The role of interactive soil moisture in land drying under anthropogenic warming. *Geophysical Research Letters* **50**, e2023GL105308 (2023).

[47] Berg, A. *et al.* Land–atmosphere feedbacks amplify aridity increase over land under global warming. *Nature Climate Change* **6**, 869–874 (2016).

[48] Insua-Costa, D. *et al.* Structural warming biases distort extreme rainfall intensification estimates in event attribution. *EGUsphere* **2026**, 1–24 (2026).

[49] Dong, W. *et al.* Contrasting response of mesoscale convective systems occurrence over tropical land and ocean to increased sea surface temperature. *Geophysical Research Letters* **51**, e2024GL109251 (2024).

[50] Dunkl, I., Bastos, A. & Sippel, S. European summer drying largely driven by atmospheric circulation changes since the 1980s. *Nature Geoscience* 1–8 (2026).

[51] Bakels, L. *et al.* FLEXPART version 11: Improved accuracy, efficiency, and flexibility. *Geoscientific Model Development* **17**, 7595–7627 (2024).

[52] Deman, V. M. H., Insua-Costa, D., Keune, J., Koppa, A. & Miralles, D. G. A four-decade global Lagrangian air-parcel trajectory dataset for atmospheric moisture and heat analysis. *Earth System Science Data* **18**, 4593–4615 (2026).

[53] Insua-Costa, D., Deman, V. M. H. & Miralles, D. G. Heat And MoiSture Tracking framEwoRk version 2.0 (HAMSTER v2) (2.0.0). *Zenodo* (2026). URL https://doi.org/10.5281/zenodo.20181215.

[54] Li, H. *et al.* Observational evidence of compensatory influences of deforestation on downwind precipitation in Brazilian breadbaskets. *npj Climate and Atmospheric Science* **8**, 279 (2025).

[55] Deman, V. M. H., Insua-Costa, D. & Miralles, D. G. FLEXPART v11 Global Trajectory Dataset (1979–2024) [Data set]. *Zenodo* (2025). URL https://doi.org/10.5281/zenodo.17952362.

Supplementary Files

This is a list of supplementary files associated with this preprint. Click to download.

- Supplementarypaper2.pdf